

# Thermal Characterization of Micrometric Polymeric Thin Films by Photoacoustic Spectroscopy

Mareny Guadalupe Fernández-Olaya, Adriana Paola Franco-Bacca, Pablo Genaro Martínez-Torres, Miguel Angel Ruiz-Gómez, David Meneses-Rodríguez, Roberto Li Voti, and Juan José Alvarado-Gil\*

In materials science, the knowledge of the thermal properties of thin films on thick substrates is crucial in determining the role of the film in the physical properties of the entire system. Even though the role of the film can be very important, the determination of its thermal properties is a challenging task due to the fact that its contribution to heat transfer is generally hard to single out from the influence of the substrate. Herein, a simple analytical methodology, based on the photoacoustic technique, useful in the thermal characterization of thin films on thick substrates, is presented. The approach is based on illuminating one side of the substrate with a modulated laser beam and monitoring the thermal contrast when a thin film is formed on the opposite side. This methodology allows to unambiguously determine the volumetric heat capacity of micrometric polymeric thin films. The limits of applicability of the method as well as the possibility of performing a full characterization of the thermal properties of the film are discussed.

## 1. Introduction

The determination of the thermal properties of thin films and coatings is crucial in a broad range of applications, which require the knowledge of how the heat can be stored, transferred, or removed from the surface of a material.<sup>[1–4]</sup> Photothermal spectroscopies have shown to be very useful in studying the optical and thermal properties of films.<sup>[5,6]</sup> These methodologies are based on the analysis of the temperature field, generated by heating the material by either modulated or pulsed light sources.<sup>[7]</sup> The associated changes in temperature are measured by different techniques based on optical, acoustic, and thermal methods.<sup>[5,7]</sup> In the case of frequency domain methodologies, involving modulated light sources, the spatial resolution of the temperature field is of the order of the thermal diffusion length  $\mu = (\alpha/\pi f)^{1/2}$ , where  $\alpha$  is the thermal diffusivity of the material and  $f$  is the frequency.<sup>[7]</sup> In particular, photoacoustics (PA), in which the changes of temperature are monitored by acoustic microphones,<sup>[6]</sup> has been used to analyze low-thermal-diffusivity thin films with micrometric and submicrometric thickness, using frequencies up to some tenths of KHz.<sup>[8–10]</sup> In the case of SiO<sub>2</sub> films, the authors reported that they can determine the thermal conductivity with a maximum error of 15%, in which the error bars grow when the thickness of the film diminishes.<sup>[8]</sup> For polymer films, Hermann et al. performed a careful analysis of the sensitivity of the PA technique and have associated uncertainties in the thermal conductivity, which are in the range of 6%–10%.<sup>[9,10]</sup> Similarly, using photothermal radiometry, monitoring the thermal wave effects by the emitted thermal radiation has been shown that it is possible to determine the thermal properties of submicrometric polymeric films with similar modulation frequencies with uncertainties of 16%.<sup>[11]</sup>


While high-frequency methodologies can yield valuable results, it is important to incorporate the roughness and corresponding optical properties in the analysis, as well as perform nontrivial noise reduction and signal extraction. Based on the previously reported findings, it would be desirable to have at hand simple low modulation frequency methodologies, which can provide thermal analysis of the films and that does not involve the direct illumination of the film. One of the possibilities

M. G. Fernández-Olaya, A. P. Franco-Bacca, J. J. Alvarado-Gil  
Applied Physics Department  
CINVESTAV, Unidad Mérida  
Km. 6 Antigua carretera a Progreso Apdo. Postal 73, Cordemex, Mérida,  
Yucatán C.P. 97310, Mexico  
E-mail: juan.alvarado@cinvestav.mx

P. G. Martínez-Torres  
Institute of Physics and Mathematics  
Universidad Michoacana de San Nicolás de Hidalgo  
Edificio C-3, Cd. Universitaria, Morelia, Michoacán C.P. 58040, Mexico

M. A. Ruiz-Gómez, D. Meneses-Rodríguez  
CONACYT-Applied Physics Department  
CINVESTAV, Unidad Mérida  
Km. 6 Antigua carretera a Progreso Apdo. Postal 73, Cordemex, Mérida,  
Yucatán C.P. 97310, Mexico

R. Li Voti  
Dipartimento di Scienze di Base e Applicate per l'Ingegneria  
Sapienza Università di Roma  
Via Antonio Scarpa 16, 00161 Rome, Italy

 The ORCID identification number(s) for the author(s) of this article can be found under <https://doi.org/10.1002/pssr.202300057>.

© 2023 The Authors. physica status solidi (RRL) Rapid Research Letters published by Wiley-VCH GmbH. This is an open access article under the terms of the Creative Commons Attribution-NonCommercial License, which permits use, distribution and reproduction in any medium, provided the original work is properly cited and is not used for commercial purposes.

DOI: 10.1002/pssr.202300057

in photothermal science, which deserves to be explored, involves the use of thermal contrast between adjacent layers, which could be used to increase the spatial resolution at low modulation frequencies, as has been discussed in the literature.<sup>[12,13]</sup>

Otherwise, PA has shown to be a valuable technique in studying the time evolution of the physical properties of diverse systems, including polymerization, sedimentation, diffusion, among others.<sup>[14–16]</sup> Moreover, the real-time monitoring of the formation of polymeric layers from liquid solution has opened the possibility of detecting the presence of thin films of a few micrometers, on substrates of hundreds of micrometers, using modulation frequencies under 100 Hz, in agreement with previous studies based on thermal waves interference.<sup>[17,18]</sup>

In this article, the possibility of broadening the capacity of the low-frequency PA methodologies, aimed to establish a simple method to perform the thermal characterization of films with a thickness of the order of a few micrometers deposited on thick substrates, is explored. In our methodology, it is shown that using a conventional PA cell allows to unambiguously determine the volumetric heat capacity of a thin film, by illuminating at low modulation frequency one face of the substrate, while the film is deposited on the opposite one.

## 2. Theory

Let us consider a two-layer system, with thickness  $l_1$  and  $l_2$  respectively, surrounded by air as shown in **Figure 1**. A light source with amplitude  $I$  and harmonically modulated at a frequency  $f$  uniformly illuminates the surface of the layer 1, inducing thermal waves in the whole sample. If the area of light incidence is large enough, the 1D heat transport in the layered system can be assumed.

The temperature at  $x = 0$  (i.e., the illuminated side of layer 1) can be determined by solving the corresponding heat diffusion equation, imposing the continuity of temperature and heat flux at each interface. Additionally, assuming that layer 1 is opaque and neglecting the air thermal effusivity, in comparison with the corresponding values of the layers, it can be shown that the temperature is given by<sup>[14,19]</sup>

$$T_{21}(x = 0, l_2, f) = \frac{I}{k_1 \sigma_1} \frac{1 + R_S \cdot \exp(-2\sigma_1 l_1)}{1 - R_S \cdot \exp(-2\sigma_1 l_1)} \quad (1)$$

with

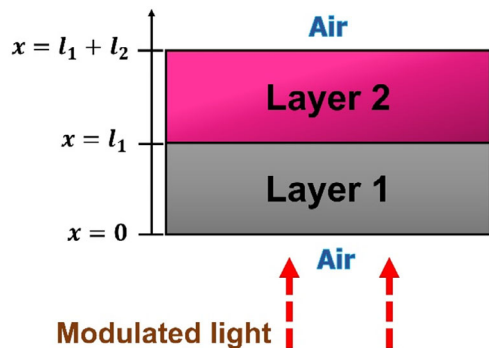


**Figure 1.** Schematic diagram of the analyzed two-layer system.

$$R_s = \frac{R_{21} + \exp(-2\sigma_2 l_2)}{1 + R_{21} \cdot \exp(-2\sigma_2 l_2)}, \quad R_{21} = \frac{1 - \frac{e_2}{\alpha_1}}{1 + \frac{e_2}{\alpha_1}}, \quad \text{and} \quad (2)$$

$$\sigma_m = (1 + i) \sqrt{\frac{\pi f}{\alpha_m}}$$

where  $k_1$  is the thermal conductivity of layer 1,  $e_m, \alpha_m$ , ( $m = 1, 2$ ) are the thermal effusivity and thermal diffusivity of layers 1 and 2, respectively, and  $i = \sqrt{-1}$ . Thermal boundary resistance between layers 1 and 2 is here neglected.

In the proposed methodology, layer 1 is the reference bare substrate with fixed thickness  $l_1$ , while the thickness  $l_2$  of layer 2 changes depending on the growing process. Therefore, the temperature at  $x = 0$  of the bare substrate without any deposition can be used as a normalization function as follows

$$T_{\text{ref}}(x = 0, f) = \frac{I}{k_1 \sigma_1} \frac{1 + \exp(-2\sigma_1 l_1)}{1 - \exp(-2\sigma_1 l_1)} \quad (3)$$

The normalized temperature at the front surface, obtained from the ratio of the temperatures given by Equation (1) and (3), is given by

$$T_N(x = 0, l_2, f) = \frac{T_{21}}{T_{\text{ref}}} = \left[ \frac{1 + R_S \cdot \exp(-2\sigma_1 l_1)}{1 - R_S \cdot \exp(-2\sigma_1 l_1)} \right] \cdot \left[ \frac{1 - \exp(-2\sigma_1 l_1)}{1 + \exp(-2\sigma_1 l_1)} \right] \quad (4)$$

To determine the conditions in which the experiments should be performed to be able to extract the thermal properties from the temperature, simulations of Equation (4) as a function of the thickness of layer 2 were performed. Layer 1 is fixed having a thickness of 100  $\mu\text{m}$ , with the thermal properties of 304-stainless steel ( $\alpha = 3.68 \times 10^{-6} \text{ m}^2 \text{ s}^{-1}$ ,  $e = 7631 \text{ W s}^{1/2} \text{ m}^{-2} \text{ K}^{-1}$ ).<sup>[20]</sup>

These analyses were performed for several polymeric materials, having a long range of thermal properties, and for aluminum oxide ( $\text{Al}_2\text{O}_3$ ), which has a much higher thermal diffusivity, in order to compare with the polymers (see **Table A1**).<sup>[20]</sup> Numerical simulations of Equation (1) for materials listed in Table A1 are shown in **Figure 2**. Even if the thermal diffusivity of  $\text{Al}_2\text{O}_3$  is much larger than the polymers one, it can be observed that there are not strong differences between the  $\text{Al}_2\text{O}_3$  and the polymer temperature curves. In contrast, when the volumetric heat capacity varies, noticeable differences between temperature curves are observed.

The normalized temperature does not follow a simple behavior on only one of the thermal properties. The curves with the higher absolute values of the slope correspond to polyimide resin, followed by polystyrene, oil, PMMA, and  $\text{Al}_2\text{O}_3$ . However, at this point, the dependence on the whole set of thermal properties is not easy to single out. To explore these aspects an analysis, based on an approximation for very small thickness, of the expression for the normalized temperature is performed. Figure 2b shows a closer look at this dependence for small thicknesses of the upper layer 2. The curves which are closer have similar values for volumetric heat capacity, concluding that for thinner layers,  $\rho C$  is the dominant parameter and exhibits a nearly linear behavior.

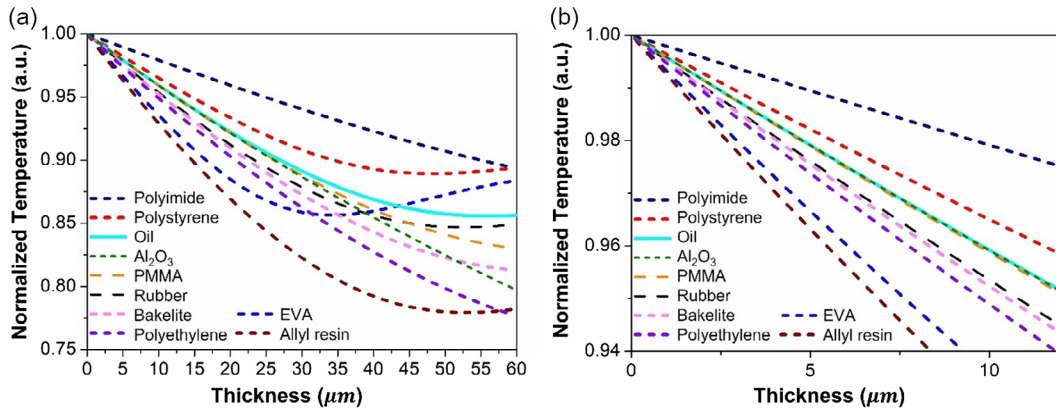


**Figure 2.** Simulated normalized temperature as a function of the thickness  $l_2$  for different kinds of materials. Modulation frequency has been kept at 7 Hz: a) thickness range from 0 to 60  $\mu\text{m}$  and b) zoom-in from 0 to 12  $\mu\text{m}$ .

The key idea of our approach is to analyze the case when layer 2 is thermally thin, using the McLaurin expansion truncated up to a second order for the exponential term in the quantity  $R_s$  of Equation (1), as follows (see Appendix for more details).

$$\exp(-2\sigma_2 l_2) = 1 - 2\sigma_2 l_2 + 2\sigma_2^2 l_2^2 + \dots \quad (5)$$

From Equation (A18), the amplitude of the normalized temperature difference between the two layer and the one-layer system at the front face can be expressed as

$$\Delta T_N = 4(1+i)\sqrt{\pi f} \rho_2 C_2 \frac{l_2}{e_1} \cdot \frac{\exp(-2\sigma_1 l_1)}{1 - \exp(-4\sigma_1 l_1)} \times \left[ 1 - (1+i)\sqrt{\pi f} \rho_2 C_2 \frac{l_2}{e_1} \cdot \coth(\sigma_1 l_1) \right] \quad (6)$$

To determine the accuracy of the approximation (Equation (6)), compared with the exact expression (Equation (4)), with  $\Delta T_N = 1 - T_N$ , simulation of the behavior of the temperature for the polymers, given in Table A1, was performed. The results are presented in **Figure 3**. A good agreement

between the complete and approximated expressions is shown in **Figure 3**, for thickness smaller than 25  $\mu\text{m}$ , for materials with thermal diffusivities smaller than  $0.25 \times 10^{-6} \text{ m}^2 \text{ s}^{-1}$ . In contrast, for materials with larger thermal diffusion length, as  $\text{Al}_2\text{O}_3$ , for which  $\alpha = 10.3 \times 10^{-6} \text{ m}^2 \text{ s}^{-1}$ , the deviation is notable, and our approximated expression is not valid anymore.

### 3. Experimental Section

In this section, the basic ideas of the approach introduced previously, were used to perform the thermal characterization of polymeric films produced by simple evaporation. The growth of the films was monitored using the method developed by Martinez-Torres et al.<sup>[14]</sup> The experimental setup is shown in **Figure 4** and **5**. A 100  $\mu\text{m}$  304-stainless steel plate was used as a substrate. This substrate was heated periodically by a laser beam having a cross section with a diameter ( $d$ ) of 7.6 mm passing through the quartz window, which generated the thermal waves in the layered system, inducing pressure changes in the air enclosed in the PA chamber, which was detected by an electret microphone. On top of the steel substrate a plastic ring was

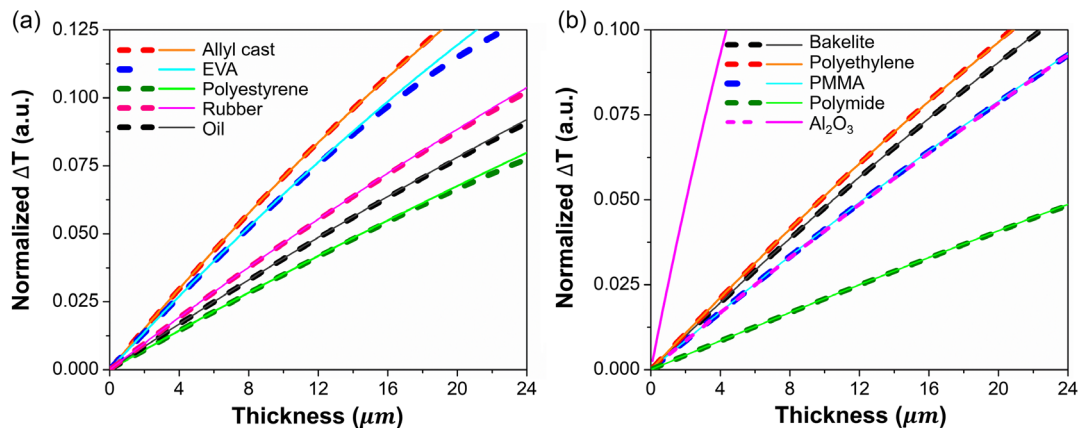


**Figure 3.** Comparison between normalized temperature, as a function of the thickness of layer 2, for the complete equation (Equation (4), dashed line) and the approximated expression (Equation (6), continuous line) a) for diffusivities lower than  $0.1 \times 10^{-6} \text{ m}^2 \text{ s}^{-1}$ , b) for diffusivities between  $0.11 \times 10^{-6} \text{ m}^2 \text{ s}^{-1}$  and  $10.3 \times 10^{-6} \text{ m}^2 \text{ s}^{-1}$ .

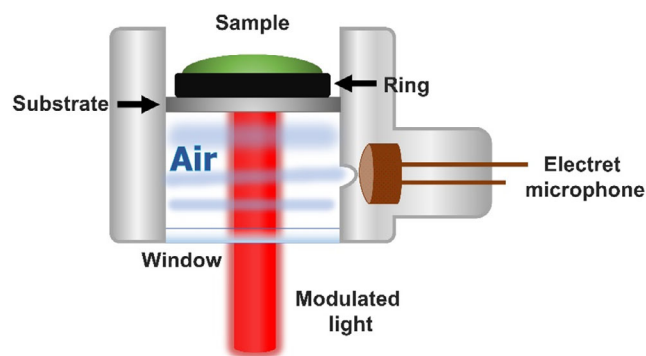


**Figure 4.** Schematic diagram of the PA cell.

attached (7.6 mm inside diameter and 1 mm in thickness) and used to form the container of the liquid sample.

A schematic diagram of the experimental setup to analyze the development of the thin polymeric films is presented in Figure 5. The general idea was to put a drop of the polymer solution inside the container on top of the substrate, closing the upper part of the PA cell. After that, the solvent was let to evaporate for several hours in atmospheric conditions, while monitoring the stability of the PA signal to guarantee a good measurement. Slow evaporation, favors for some polymers, the formation of uniform layers. To guarantee good absorbance of the incident modulated light on the steel substrates, its face on which the laser beam will be impinged was previously covered with a very thin layer (10  $\mu\text{m}$  of aerosolized graphite (Ted Pella Inc.)) and then placed on top of the PA cell.

Two types of polymeric films were studied: potato starch biopolymers and PEDOT: PSS. Starch biopolymer films were synthesized through the casting method. A homogeneous solution of 0.24 g of potato starch (Sigma-Aldrich) diluted in 30 mL of distilled and deionized water (DDW) was prepared and mixed with different amounts of sorbitol (Sigma-Aldrich, 98%). This mixture was heated and stirred at 40  $^{\circ}\text{C}$  and 400 rpm for

10 min to homogenize it. Then, the temperature was increased 5  $^{\circ}\text{C min}^{-1}$  until reaching the starch gelation point at 80  $^{\circ}\text{C}$ .<sup>[21]</sup> Sorbitol was used as a plasticizer, because it facilitates the crosslinking between the main starch polymer chains.<sup>[22]</sup> Three different sorbitol volume fractions (vf%) were tested, 0.6, 0.8, and 1 vf%.

PEDOT:PSS (1.3 wt% dispersions in water, Sigma-Aldrich) was further diluted in water for 10%, 33%, and 55%. In order to reach larger polymer fractions, PEDOT:PSS liquid samples were also prepared using isopropyl alcohol ( $\geq 99.9\%$ , Fermont), obtaining samples of 60%, 70%, 80%, and 90%.

The illuminating beam was generated using a 100 mW diode laser at 633 nm (HL63163DG) modulated at constant frequency ( $f = 7$  Hz), and sent onto the substrate, while monitoring the PA signal on the illuminated side of the sample. The microphone signal was sent into a lock-in amplifier (SR830), and the data acquisition was made with a homemade LabVIEW-based program (see Figure 5). When the PA signal was stable, starch-based biopolymer (40  $\mu\text{L}$ ) or diluted PEDOT: PSS solutions (100  $\mu\text{L}$  for samples diluted in water and 50  $\mu\text{L}$  for samples diluted in isopropyl alcohol) were dropped on the steel substrate and the PA signal was recorded as a function of time in a similar way reported by Martínez-Torres et al.<sup>[14]</sup>

## 4. Result and Discussion

**Figure 6** shows three typical results of the measurements of the PA amplitude as a function of time, for each kind of system. The dynamic evolution of the system can be very complex, due to its dependence on the evaporation rate, changes in solute concentration, and formation of meniscus and agglomerates, among several others.<sup>[14]</sup> However, in general, the PA amplitude shows a pattern, in such a way that when the liquid sample is initially deposited, the signal decreases and remains almost constant ( $T_i$ ) up to a time at which a minimum appears. This minimum is related to the thermal wave interference process occurring when

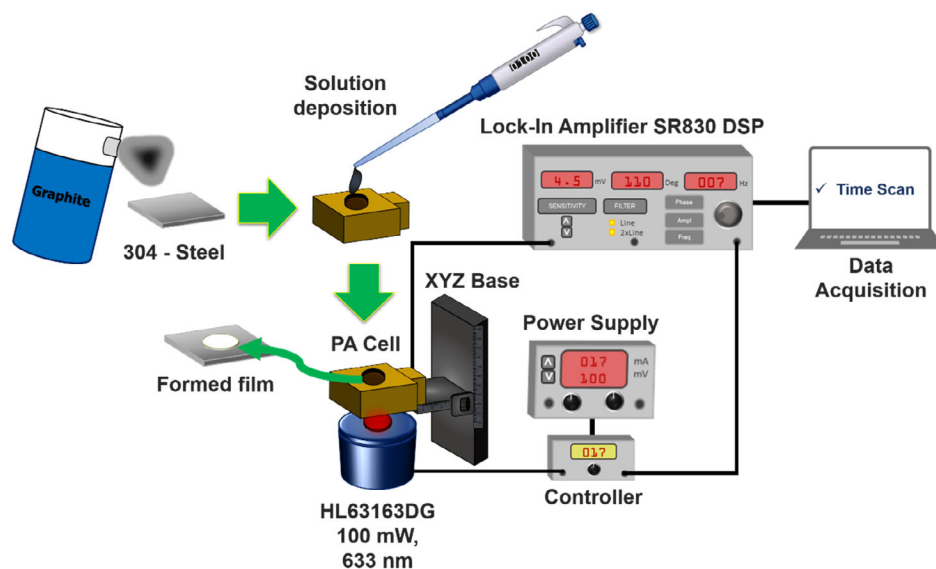


**Figure 5.** Experimental arrangement used for the PA measurements.

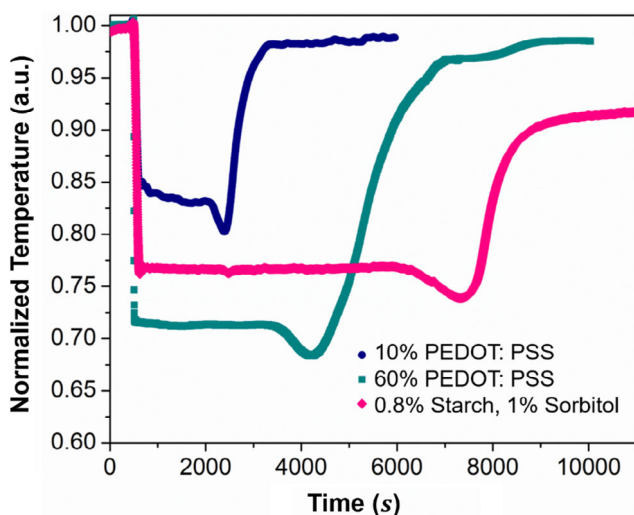


**Figure 6.** Normalized PA amplitude as a function of thickness for a starch biopolymer, as well as for samples with 10% PEDOT:PSS diluted in water, and 60% PEDOT:PSS diluted in isopropyl alcohol.

the thickness of the sample is of the order of the thermal diffusion length  $\mu = (\alpha/\pi f)^{1/2}$ .<sup>[23,24]</sup> Afterward, a sudden increase occurs corresponding to the final stage of the evaporation process. During the last stage, in which all the solvent nearly evaporates, the film is formed, and the amplitude of the PA signal becomes constant ( $T_f$ ).

In order to determine the thermal properties of the polymer films, we only need to consider the difference  $\Delta T_N$  between the final amplitude, when the polymer film is completely formed (when the solvent is completely evaporated), and the initial amplitude of the substrate without the liquid sample. The experimental data will be analyzed using the exact and the approximated expressions given by Equation (4) and (6) respectively.

It is important to mention that our methodology provides the real-time monitoring of the temperature when the film is growing. This implies changes on several factors including geometry and thickness of the film as stated before. Evaporation of the solvent can also produce other observable effects, due to the fact that the pressure inside the PA cell depends on the nonmodulated temperature of the cell.<sup>[5,7,25–27]</sup> However, in our case the evaporation process is very slow, it takes several thousands of seconds. Therefore, it is possible to reach the thermalization of the cell with the ambient temperature and in consequence keeping nearly constant the nonmodulated temperature of the PA cell. In fact, performing experiments with solvents with fast evaporation rates generates observable effects in the PA cell signal. Having these restrictions in mind in our experiments, we avoided those situations, using long evaporation solvents. Additionally, in the methodology presented here, to determine the thermal properties of the films, it is not necessary to consider the changes in nonmodulated temperature and evolution of the thickness of layer 2, because we only need to analyze the last stage in which the evaporation of the solvent ended and the films are formed and the nonmodulated temperature is stable.

Considering that our objective is to determine the thermal properties of the polymer, the thickness of the final formed

samples was measured by analyzing the cross section of the system sample-substrate using scanning electron microscopy (SEM). To obtain these images, the polymer films were coated with a layer of 170 nm of silver, which allows to prevent the peeling off of the polymer film from the substrate, when the sample is cut. **Figure 7** shows representative SEM images of the polymer films observing that the thicknesses are in the range of micrometers. The results indicate that the thickness of the PEDOT:PSS film increases with the concentration of the solution.

Based on the cross section of the SEM images, it can be inferred that the uncertainty on the thickness is around 0.5  $\mu\text{m}$ . It is important to mention that the thermal expansion can induce a change of the thickness of the formed film. However, we took into account that in the final stage, we have a two-layer system formed by a polymer film on a steel substrate, with an estimated thermal expansion coefficient of around  $2 \times 10^{-4} \text{K}^{-1}$ .<sup>[28]</sup> Due to the fact that the increase of the temperature during the PA experiments, induced by the heating of the laser light, is at the most a few centigrade degrees, the changes in the thickness are much smaller than the uncertainty of 0.5  $\mu\text{m}$ . Interestingly according to our results, shown in **Figure 6** and **Table 1**, thinner samples produce smaller changes in  $\Delta T_N$ . It can be inferred that, in our experiments, having thinner films than 1  $\mu\text{m}$  would hardly generate an observable change in  $\Delta T_N$ .

On the other hand, the substrate was characterized by X-ray diffraction (XRD) analysis confirming that its crystal structure corresponds to 304 stainless steel ( $\text{Fe}_{0.49}\text{Cr}_{0.29}\text{Ni}_{0.16}\text{C}_{0.06}$ ; PDF 00-033-0397).<sup>[29]</sup> Therefore, it is possible to use the physical properties of this material in our models (Equation (4) and (6)). The thermal properties for this well-known material were taken from the Materials Thermal Properties Database.<sup>[20]</sup> These are  $\alpha = 3.68 \times 10^{-6} \text{m}^2 \text{s}^{-1}$ ,  $e = 7631 \text{Ws}^{1/2} \text{m}^{-2} \text{K}^{-1}$ ,  $k = 14.64 \text{Wm}^{-1} \text{K}^{-1}$ .

Based on these values, the first factor of Equation (6) depends only on the parameters of the substrate and modulation frequency (7 Hz), and therefore

$$\text{Abs} \left( \frac{4 \exp \left[ -2(1+i) \frac{l_1}{\mu_1} \right]}{e_1 \left( 1 - \exp \left[ -4(1+i) \frac{l_1}{\mu_1} \right] \right)} \right) = 3.80 \times 10^{-4} \text{W m}^2 \text{Ks}^{-1/2} \quad (7)$$

Hence, at first-order approximation in the thickness of layer 2, Equation (6), becomes

$$\Delta T_N \approx 4(1+i) \sqrt{\pi f} \rho_2 C_2 \frac{l_2}{e_1} \cdot \frac{\exp(-2\sigma_1 l_1)}{1 - \exp(-4\sigma_1 l_1)} \quad (8)$$

Interestingly, this equation implies that the absolute value of the temperature is mainly governed by the volumetric heat capacity ( $\rho_2 C_2$ ) of layer 2, when this layer is very thin.

A special case occurs if the substrate (layer 1) was thermally thin, where a further simplification could be done as

$$\Delta T_N = \frac{\sigma_2 l_2 e_2}{\sigma_1 l_1 e_1} = \frac{\rho_2 C_2 l_2}{\rho_1 C_1 l_1} \quad (9)$$

Additionally, from the data shown in **Figure 3**, the linear approximation, stated in Equation (8), is clearly not followed

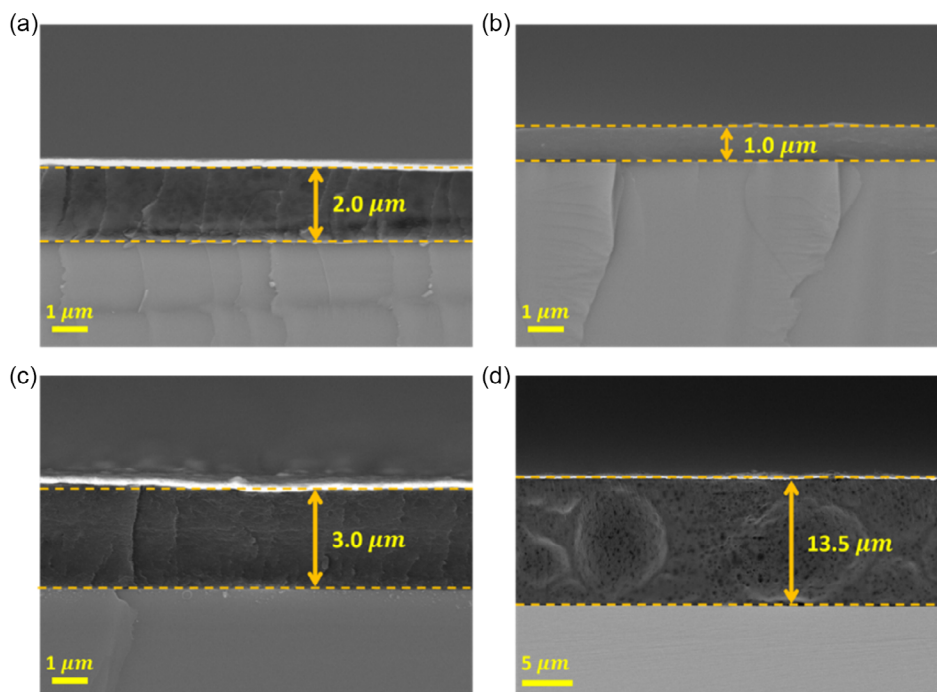


**Figure 7.** Representative SEM images of cross section of the formed polymers after the solvent evaporation for a) 10% PEDOT: PSS diluted in water, b) 60% PEDOT: PSS and c) 70% PEDOT:PSS both diluted in isopropyl alcohol, and d) starch biopolymer (1% sorbitol). SEM analysis was performed using a field-emission microscope (FESEM-JEOL-7600F) with a LABE detector of 10.0 kV.

**Table 1.** Thermal properties for PEDOT:PSS and starch biopolymer films obtained from the fitting properties of the experimental data presented in Figure 8.

Concentration [%]	$\Delta T_N$ ( $\pm 0.001$ )	$l_2$ ( $\pm 0.5 \times 10^{-6} \text{m}$ )	$\rho_2 C_2$ [ $\times 10^6 \text{Jm}^{-3} \text{K}^{-1}$ ] Using Equation (8)	$e_2$ [ $\text{Ws}^{1/2} \text{m}^2 \text{K}^{-1}$ ] Using Equation (4)
<b>PEDOT:PSS diluted in water</b>				
10%	0.020	2.0		
33.3%	0.028	3.0	$4.10 \pm 0.38$	$900 \pm 40$
50%	0.056	5.5		
<b>PEDOT:PSS diluted in isopropyl alcohol</b>				
60%	0.012	1.0	$4.54 \pm 0.41$	$900 \pm 90$
70%	0.037	3.0		
80%	0.090	8.0		
90%	0.140	12.5		
<b>Starch-based biopolymer</b>				
0.8%, 0.6%	0.040	6.5		
0.8%, 0.8%	0.050	8.0	$2.49 \pm 0.46$	$1100 \pm 100$
0.8%, 1.0%	0.084	13.5		

when increasing the thickness of layer 2. Considering that our samples are very thin, the analysis of the experimental data was performed starting with the first order-approximation (Equation (8)). As can be seen in **Figure 8**, the fitting using the linear approximation is adequate and provided the values

of the volumetric heat capacities of PEDOT: PSS and starch films, which agree with the values reported in the literature.<sup>[14,20]</sup> Even though the fittings using Equation (8) are good, we wanted to explore the viability of obtaining additional information from our measurements. Therefore, we use the exact solution (Equation (4)) to fit the experimental data, taking the thermal effusivity as free parameter, considering that thermal diffusivity would be in the order of  $0.1 \times 10^{-6} \text{m}^2 \text{s}^{-1}$ . The data is also well fitted (see Figure 8), providing a reasonable standard deviation for the thermal effusivity (see Table 1). However, the range of thickness studied is not enough to provide an unambiguous and accurate process to determine the thermal diffusivity, but only a rough estimation, which is related to the fact that the thermal diffusion length of the thermal waves is much larger than the thickness of the polymer films. This suggests that the heat transport in films, of a few micrometers or less, is dominated by the thermal contact between the substrate and the film. In a more specific way, the temperature  $\Delta T_N$  is closely related to the volumetric heat capacity and has minor dependence of the thermal effusivity of the film.

PEDOT: PSS films grown in isopropyl alcohol show higher values for the volumetric heat capacity than samples synthesized in water. This behavior can be related to changes in the microstructure generated by the different growth conditions, which modify the way in which the PEDOT: PSS films store heat.<sup>[18,30–32]</sup>

To understand the convergence of the series expansion to approximate to the exact solution, the analysis of the nonlinear approximation (Equation (6)) and the exact solution

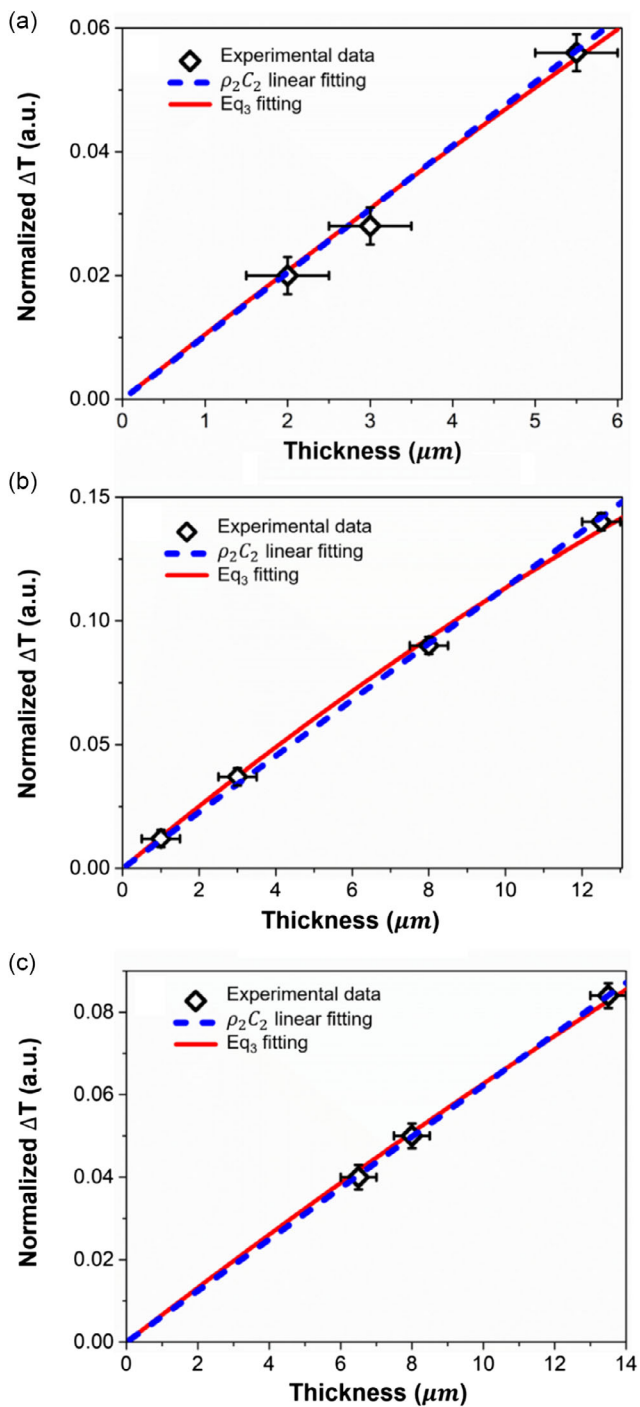


**Figure 8.** Normalized  $\Delta T$  amplitude fitting as a function of thickness for a) PEDOT: PSS diluted in water, b) isopropyl alcohol, and c) for the starch biopolymer.

(Equation (4)) is performed, for both types of polymers. Equation (6) corresponds to a second-order approximation, and it could be expected that a reasonable result can be obtained for thin films. The temperature difference for both solutions is presented in **Figure 9**, as a function of the film thickness for starch and PEDOT:PSS, taking the values  $\alpha_{\text{PEDOT:PSS}} = 4 \times 10^{-8} \text{ m}^2 \text{ s}^{-1}$ ,

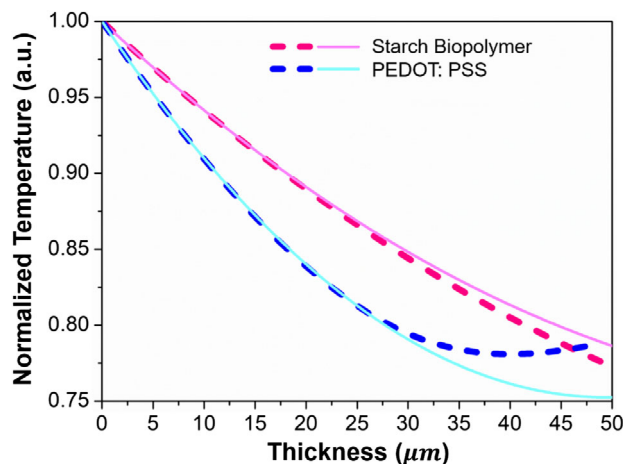


**Figure 9.** Comparison of normalized amplitude for PEDOT:PSS and starch Biopolymer, for less than 5% of deviation in  $T_N$  for increasing thickness. Dashed lines represent the complete expression (Equation (4)), and continuous lines correspond to our second-order approximation (Equation (6)).

$(\rho C)_{\text{PEDOT:PSS}} = 4 \times 10^6 \text{ J m}^{-3} \text{ K}^{-1}$ ,  $\alpha_{\text{Starch BP}} = 20.5 \times 10^{-8} \text{ m}^2 \text{ s}^{-1}$ , and  $(\rho C)_{\text{Starch BP}} = 2.49 \times 10^6 \text{ J m}^{-3} \text{ K}^{-1}$ . **Figure 9** shows that the difference between the exact and second-order approximation solution is notable even for small film thickness. This indicates that the procedure that we have chosen, consisting of using the linear approximation for very thin films and the complete equation to fit the experimental data for the effusivity when the thickness is slightly increased, is the right one. This is due to the slow convergence of the series expansion. Additionally, the ranges of thickness for the validity of the second-order approximation are wider in starch than for PEDOT:PSS. As shown in **Figure 9**, a deviation of 5% between exact and approximated curves for PEDOT:PSS occurs at 15  $\mu\text{m}$  of thickness, while for starch occurs up to 30  $\mu\text{m}$ . This is related to the fact that the thermal diffusivity is more than four times larger in starch than the value for PEDOT:PSS.

Another remarkable aspect is that we use a low-modulation frequency to perform our experiments, which guarantee working in the thermally thin region. Therefore, the dependence of the observed phenomena as well as the validity of our approach when studying this type of process requires a deeper analysis.

**Figure 10** shows the comparison of the normalized temperature as a function of the film thickness using the approximated Equation (6) and its comparison with the exact Equation (4), for different values of the modulation frequency. It was assumed that the thermal diffusivity of a polymer is typically around  $10^{-8} \text{ m}^2 \text{ s}^{-1}$ , and the thermal effusivity is of the order of  $1000 \text{ W s}^{1/2} \text{ m}^2 \text{ K}^{-1}$ , while the values for 304 stainless steel were taken from the literature.<sup>[20]</sup> It can be seen that the approximation works well for low frequencies, for thickness up to around ten  $\mu\text{m}$ , but it is only good for thickness of 1  $\mu\text{m}$  or less for frequencies of 20 Hz. This indicates that larger thermal diffusion lengths provide better results. Additionally, when the frequency is increased, the temperature difference ( $\Delta T_N$ ) can become so

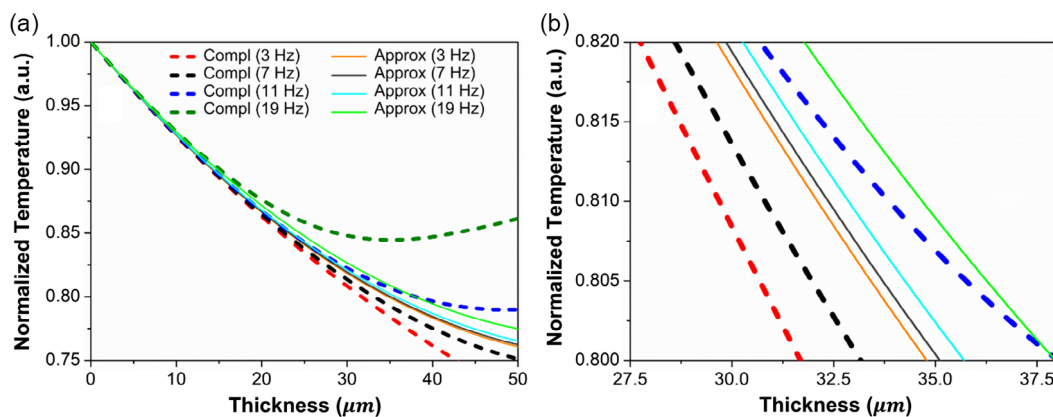


**Figure 10.** Comparison of the thickness dependence between normalized temperature for exact equation (Compl, Equation (4)) and the approximated expression (Approx, Equation (6)) for different frequencies. a) Thickness range from 0 to 50 μm and b) zoom-in from 27.4 to 37.5 μm.

small that it would be hardly measurable. We can infer that in order to have a larger range of thickness and larger changes of temperature, low frequencies can be more convenient. This is a very singular behavior because for frequencies between 7 and 10 Hz the thermal diffusion length is around 90 μm; however, our approach indicates that we can easily detect layers of a few μm. Moreover, the modulation frequency cannot be as small as we want. It is important to remark that our approach is also assuming 1D heat propagation, in consequence going to low-modulation frequencies would involve 3D effects.<sup>[33,34]</sup> In this sense, our approach must have a lower limit, which can be obtained from the criterion given by  $d \geq 10\mu$ , where  $d$  is the diameter of the laser spot and  $\mu$  is the already defined thermal diffusion length. In our case, the diameter of the laser spot is 3 mm; therefore, for the thermal diffusivities of the analyzed polymers, we have that  $10 \times 100 \mu\text{m} = 1 \text{ mm} < 3 \text{ mm}$ , and the criterion is fulfilled. However, for smaller frequencies, such as 0.5 Hz, the criterion is not satisfied.<sup>[14,32]</sup>

It is important to note that the methodology proposed in this article provides as the main result the volumetric heat capacity. For micrometric and thinner films, the proposed methodology is not enough sensitive to the thermal conductivity/diffusivity. Therefore, our technique can be even used for high-conductivity micrometric films, such as metals or diamond ones. In contrast, high-frequency methodologies, in which the film is illuminated, require very high frequencies, of the order of tenths of MHz, for studying micrometric or submicrometric high-thermal-conductivity films, with the consequent complications of the experimental methodology and data analysis.<sup>[25,33,34]</sup> Additionally, our method does not require to know the optical properties of the film and it can have a large roughness, because we illuminate the substrate, not the film. These aspects make our method much simpler, without complications of the experimental methodology and data analysis involved in high-frequency techniques. In this sense, our technique provides results for a wider range of thermal conductivity/diffusivities. However, our approach allows the determination of the thermal diffusivity, only through increasing film thickness, until the thermal diffusion length is comparable to the film thickness, as shown in Figure 10.

It is important to mention that the methodology can be improved in two aspects, the first one by generating smoother films by another growth technique, being able to get smaller values of  $\Delta l_2$ , providing more accurate values of the volumetric heat capacity. A second possibility would be to increase the sensitivity, to the presence of the formed polymer layers on top of the substrate, by introducing a lighter gas than air inside the PA chamber, which would allow to measure the required  $\Delta T_N$  and determine the volumetric heat capacity of thinner films.<sup>[9,10]</sup> Finally, it would also be interesting to develop the corresponding analysis of heat transfer phenomena in multilayered systems in a wide range of thickness of the layers to further explore the spatial resolution of photothermal techniques.

## 5. Conclusion

In this article, the heat transfer in micrometric PEDOT: PSS and starch polymer films grown on a steel substrate was monitored using the PA technique. Our theoretical and experimental results showed that the amplitude of the modulated temperature exhibits a nearly linear dependence on the thickness of the formed film, when this thickness was under 10 μm. This dependence allows to determine the volumetric heat capacity using a first-order approximation of the theoretical expression of the modulated temperature and to perform an estimation of the thermal effusivity of the film when applying the nonapproximated expression of the theoretical expression.

According to our analysis, the optimal modulation frequency of our technique is around a few Hz, keeping in mind that the frequency cannot be too low because the 3D heat transfer effects must be taken into account, but cannot be too high because, in this case the temperature difference ( $\Delta T_N$ ) would be too small and in consequence hardly measurable. Our findings demonstrate that thermal contrast is an effective method for analyzing heat transfer in polymer films, when the sample is heated by illuminating the substrate on which the polymer is deposited. The method, proposed in this article, enables the study of thermal properties in thin films without the need for high-modulation frequencies or prior knowledge of the film's roughness or optical properties.



## Appendix

Thermal properties used for numerical simulation of the behavior of the modulated temperature for different polymers are presented in **Table A1**.

A second-order series expansion was performed in the exponential

$$\exp(-2\sigma_2 l_2) = 1 - 2\sigma_2 l_2 + 2\sigma_2^2 l_2^2 + \dots \quad (\text{A1})$$

The coefficient  $R_s$  is given by

$$R_s = \frac{R_{21} + 1 - 2\sigma_2 l_2 + 2\sigma_2^2 l_2^2}{1 + R_{21} - 2\sigma_2 l_2 R_{21} + 2\sigma_2^2 l_2^2 R_{21}} \quad (\text{A2})$$

$$R_s = \left( \frac{1 + R_{21} - 2\sigma_2 l_2 + 2\sigma_2^2 l_2^2}{1 + R_{21}} \right) \left[ \frac{1}{1 - \frac{R_{21}}{1+R_{21}} (2\sigma_2 l_2 - 2\sigma_2^2 l_2^2)} \right] \quad (\text{A3})$$

Applying a McLaurin approximation for the second factor, and keeping in mind that

$$\frac{1}{1-z} \approx 1 + z + z^2 \text{ for } z \ll 1, \text{ one obtains}$$

$$R_s = \left( 1 - \frac{2\sigma_2 l_2 - 2\sigma_2^2 l_2^2}{1 + R_{21}} \right) \left[ 1 + \frac{R_{21}}{1 + R_{21}} (2\sigma_2 l_2 - 2\sigma_2^2 l_2^2) + \left( \frac{R_{21}}{1 + R_{21}} \right)^2 (2\sigma_2 l_2 - 2\sigma_2^2 l_2^2)^2 \right] \quad (\text{A4})$$

after some algebra and keeping only terms in  $\sigma_2 l_2$  up to the second order

$$R_s = \left\{ 1 - \frac{1 - R_{21}}{1 + R_{21}} (2\sigma_2 l_2 - 2\sigma_2^2 l_2^2) + \left[ -\frac{R_{21}}{(1 + R_{21})^2} + \left( \frac{R_{21}}{1 + R_{21}} \right)^2 \right] 4\sigma_2^2 l_2^2 \right\} \quad (\text{A5})$$

from which

**Table A1.** Thermal properties of different of low-thermal-diffusivity polymeric materials. In the last row the thermal properties of  $\text{Al}_2\text{O}_3$  are shown as a reference of a relatively high-thermal-diffusivity material.<sup>[20]</sup>

Material	$\alpha$ ( $\times 10^{-6} \text{m}^2 \text{s}^{-1}$ )	$\rho C$ ( $\times 10^6 \text{Jm}^{-3} \text{K}^{-1}$ )	$e$ ( $\text{Ws}^{1/2} \text{m}^{-2} \text{K}^{-1}$ )
Ethyl vinyl acetate	0.03	2.76	478
Polystyrene	0.06	1.45	355
Natural rubber	0.07	1.95	516
Allyl cast resin	0.07	3.05	807
Lubricating oil	0.08	1.70	483
Bakelite	0.11	2.00	663
PMMA Poly (methyl methacrylate)	0.12	1.72	596
Polyethylene (medium density)	0.19	2.15	937
Polyimide resin	0.25	0.85	425
$\text{Al}_2\text{O}_3$	10.3	1.7	5456

$$R_s = \left[ 1 - 2 \frac{1 - R_{21}}{1 + R_{21}} \sigma_2 l_2 + 2 \left( \frac{1 - R_{21}}{1 + R_{21}} \right)^2 \sigma_2^2 l_2^2 \right] = 1 - 2\gamma + 2\gamma^2 \quad (\text{A6})$$

$$\text{where } \gamma = \frac{1 - R_{21}}{1 + R_{21}} \sigma_2 l_2 = \frac{e_2}{e_1} \sigma_2 l_2$$

The expression in Equation (A6) can be inserted directly in Equation (1)

$$T_{21} = \frac{I}{k_1 \sigma_1} \left[ \frac{1 + (1 - 2\gamma + 2\gamma^2) \cdot \exp(-2\sigma_1 l_1)}{1 - (1 - 2\gamma + 2\gamma^2) \cdot \exp(-2\sigma_1 l_1)} \right] \quad (\text{A7})$$

$$T_{21} = \frac{I}{k_1 \sigma_1} \left[ \frac{1 + \exp(-2\sigma_1 l_1) - (2\gamma - 2\gamma^2) \cdot \exp(-2\sigma_1 l_1)}{1 - \exp(-2\sigma_1 l_1) + (2\gamma - 2\gamma^2) \cdot \exp(-2\sigma_1 l_1)} \right] \quad (\text{A8})$$

and after some algebra

$$T_{21} = \frac{I}{k_1 \sigma_1} \left[ \frac{1 + \exp(-2\sigma_1 l_1) - (2\gamma - 2\gamma^2) \cdot \exp(-2\sigma_1 l_1)}{1 - \exp(-2\sigma_1 l_1) + (2\gamma - 2\gamma^2) \cdot \exp(-2\sigma_1 l_1)} \right] \cdot \left[ \frac{1 + \exp(-2\sigma_1 l_1)}{1 - \exp(-2\sigma_1 l_1)} \right] \quad (\text{A9})$$

where

$$T_{\text{ref}}(x = 0, f) = \frac{I}{k_1 \sigma_1} \frac{1 + \exp(-2\sigma_1 l_1)}{1 - \exp(-2\sigma_1 l_1)} \quad (\text{A10})$$

$$T_{21} = \left[ \frac{1 + \exp(-2\sigma_1 l_1) - (2\gamma - 2\gamma^2) \cdot \exp(-2\sigma_1 l_1)}{1 - \exp(-2\sigma_1 l_1) + (2\gamma - 2\gamma^2) \cdot \exp(-2\sigma_1 l_1)} \right] \cdot T_{\text{ref}} \quad (\text{A11})$$

from which

$$T_N = \frac{1 - 2(\gamma - \gamma^2) \cdot \frac{\exp(-2\sigma_1 l_1)}{1 + \exp(-2\sigma_1 l_1)}}{1 + 2(\gamma - \gamma^2) \cdot \frac{\exp(-2\sigma_1 l_1)}{1 - \exp(-2\sigma_1 l_1)}} \quad (\text{A12})$$

and keeping in mind that  $\frac{1}{1+z} \approx 1 - z + z^2$  for  $z \ll 1$ , one obtains

$$T_N = \left[ 1 - 2(\gamma - \gamma^2) \cdot \frac{\exp(-2\sigma_1 l_1)}{1 + \exp(-2\sigma_1 l_1)} \right] \times \left\{ 1 - 2(\gamma - \gamma^2) \cdot \frac{\exp(-2\sigma_1 l_1)}{1 - \exp(-2\sigma_1 l_1)} + 4(\gamma - \gamma^2)^2 \cdot \left[ \frac{\exp(-2\sigma_1 l_1)}{1 - \exp(-2\sigma_1 l_1)} \right]^2 \right\} \quad (\text{A13})$$

after some algebra and keeping only terms in and up to the second order it becomes

$$T_N = 1 + \frac{-4(\gamma - \gamma^2) \cdot \exp(-2\sigma_1 l_1) + 4\gamma^2 \cdot \exp(-4\sigma_1 l_1)}{[1 + \exp(-2\sigma_1 l_1)][1 - \exp(-2\sigma_1 l_1)]} + 4\gamma^2 \left[ \frac{\exp(-2\sigma_1 l_1)}{1 - \exp(-2\sigma_1 l_1)} \right]^2 \quad (\text{A14})$$

which can be simplified into

$$T_N = 1 - \gamma \frac{4 \cdot \exp(-2\sigma_1 l_1)}{1 - \exp(-4\sigma_1 l_1)} + \gamma^2 \frac{4 \cdot \exp(-2\sigma_1 l_1)}{[1 - \exp(-2\sigma_1 l_1)]^2} \quad (\text{A15})$$

and keeping in mind that  $\gamma = \sigma_2 l_2 \frac{e_2}{e_1}$

$$T_N = 1 - 4\sigma_2 l_2 \frac{e_2}{e_1} \cdot \frac{\exp(-2\sigma_1 l_1)}{1 - \exp(-4\sigma_1 l_1)} + 4\sigma_2^2 l_2^2 \frac{e_2^2}{e_1^2} \cdot \frac{\exp(-2\sigma_1 l_1)}{[1 - \exp(-2\sigma_1 l_1)]^2} \quad (\text{A16})$$

which can be written in terms of temperature variation  $\Delta T_N = 1 - T_N$  as follows

$$\Delta T_N = 4\sigma_2 l_2 \frac{e_2}{e_1} \cdot \frac{\exp(-2\sigma_1 l_1)}{1 - \exp(-4\sigma_1 l_1)} \left[ 1 - \sigma_2 l_2 \frac{e_2}{e_1} \cdot \frac{1 + \exp(-2\sigma_1 l_1)}{1 - \exp(-2\sigma_1 l_1)} \right] \quad (\text{A17})$$

$$\Delta T_N = 4\sigma_2 l_2 \frac{e_2}{e_1} \cdot \frac{\exp(-2\sigma_1 l_1)}{1 - \exp(-4\sigma_1 l_1)} \left[ 1 - \sigma_2 l_2 \frac{e_2}{e_1} \cdot \coth(\sigma_1 l_1) \right] \quad (\text{A18})$$

According to Equation (A18),  $\Delta T_N$  exhibits a substantially linear behavior with the thickness  $l_2$ . The nonlinear quadratic effect is related to the term in square brackets and can be neglected only if

$$|\sigma_2 l_2 \frac{e_2}{e_1} \cdot \coth(\sigma_1 l_1)| \ll 1 \quad (\text{A19})$$

The extreme case occurs when the layer 1 is thermally thin, and consequently  $\coth(\sigma_1 l_1) \approx 1/\sigma_1 l_1$  drastically increases. In order to find the maximum thickness  $l_2$ , which guarantees the linearity, Equation (A19) should be replaced by the more stringent one

$$\frac{\sigma_2 l_2 e_2}{\sigma_1 l_1 e_1} = \frac{\rho_2 C_2 l_2}{\rho_1 C_1 l_1} \ll 1 \quad (\text{A20})$$

In our experiment, given that  $\rho_1 C_1 = 4 \times 10^6 \text{ Jm}^{-3} \text{ K}^{-1}$  for 304 – stainless steel, and since the quantity  $\rho_2 C_2$  falls also in the same range, around some units of  $1 \times 10^6 \text{ Jm}^{-3} \text{ K}^{-1}$  for most of the materials listed in Table 1 and A1, from Equation (A20), we can conclude that nonlinear effects can be definitively neglected if  $l_2 < l_1 = 100 \mu\text{m}$ .

In such a case, Equation (A18) can be truncated at the first order as follows

$$\Delta T_N = 4\sigma_2 l_2 \frac{e_2}{e_1} \cdot \frac{\exp(-2\sigma_1 l_1)}{1 - \exp(-4\sigma_1 l_1)} = \rho_2 C_2 l_2 \cdot \frac{4\sqrt{2\pi}if}{e_1} \cdot \frac{\exp(-2\sigma_1 l_1)}{1 - \exp(-4\sigma_1 l_1)} \quad (\text{A21})$$

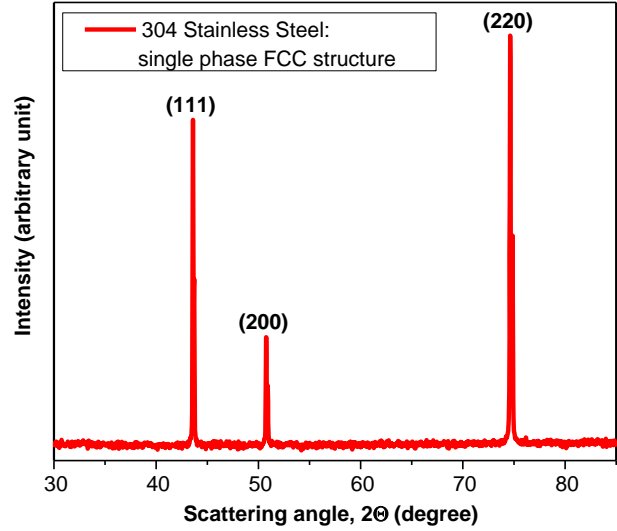


**Figure A1.** XRD pattern for 304 stainless steel substrates.

showing a clear dependence only on the volumetric heat capacity. Note that if the substrate were thermally thin a further simplification could be done so that Equation (A21) eventually becomes

$$\Delta T_N = \frac{\sigma_2 l_2 e_2}{\sigma_1 l_1 e_1} = \frac{\rho_2 C_2 l_2}{\rho_1 C_1 l_1} \quad (\text{A22})$$

X-ray diffraction spectrum of the substrate is shown in **Figure A1**, confirming 304 stainless steel material,<sup>[29]</sup> with characteristic peaks appearing at  $2\theta = 43.59^\circ, 50.75^\circ, 74.63^\circ$ .

## Acknowledgements

The authors would like to acknowledge the support of the National Council of Science and Technology of Mexico (CONACYT) through the Ph.D. scholarship of Marenly Guadalupe Fernández Olaya (CVU 706871) and grants CB-2017/2018-A1-S-21018 and PNRR MUR project PE0000023-NQSTI. Authors are also grateful for allowing us to use the facilities of LANNBIO Cinvestav-Mérida supported by the grants: FOMIX Yucatán 2008–108160, CONACYT LAB-2009-01-123913, 188345, 204822, 292692, 294643. Technical assistance of J. Bante-Guerra, D. Aguilar, and V. Rejón is also acknowledged.

## Conflict of Interest

The authors declare no conflict of interest.

## Data Availability Statement

The data that support the findings of this study are available on request from the corresponding author. The data are not publicly available due to privacy or ethical restrictions.

## Keywords

photoacoustics, thin layers, volumetric heat capacities

Received: February 10, 2023  
Revised: March 25, 2023  
Published online: April 25, 2023

- [1] D. G. Cahill, W. K. Ford, K. E. Goodson, G. D. Mahan, A. Majumdar, H. J. Maris, R. Merlin, S. R. Phillpot, *J. Appl. Phys.* **2003**, *93*, 793.
- [2] P. Peumans, A. Yakimov, S. R. Forrest, *J. Appl. Phys.* **2003**, *93*, 3693.
- [3] M. Dresselhaus, G. Chen, M. Tang, R. Yang, H. Lee, D. Wang, Z. Ren, J.-P. Fleurial, P. Gogna, *Adv. Mater.* **2007**, *19*, 1043.
- [4] Y. W. Mai, Z. Z. Yu, *Polymer Nanocomposites*, CRC Press, Cambridge, UK; Boca Raton, FL **2006**.
- [5] M. Bertolotti, R. Li Voti, *J. Appl. Phys.* **2020**, *128*, 230901.
- [6] H. Vargas, L. C. M. Miranda, *Rev. Sci. Instrum.* **2003**, *74*, 794.
- [7] D. P. Almond, P. Patel, P. M. Patel, *Photothermal Science and Techniques*, Springer Science & Business Media. London, UK, **1996**.
- [8] X. Wang, H. Hu, X. Xu, *Trans. ASME* **2001**, *123*, 138.
- [9] K. Herrmann, N. W. Pech-May, M. Retsch, *Photoacoustics* **2021**, *22*, 100246.
- [10] K. Herrmann, S. Freund, F. Eller, T. Rößler, G. Papastavrou, E. M. Herzig, M. Retsch, *Materials* **2022**, *15*, 7700.
- [11] D. Trefon-Radziejewska, G. Hamaoui, M. Chirtoc, N. Horny, V. Smokal, A. Biitseva, O. Krupka, B. Derkowska-Zielinska, *Mater. Chem. Phys.* **2019**, *223*, 700.
- [12] M. Chirtoc, J. Gibkes, H. G. Walther, A. Christ, J. S. Antoniow, D. Bicanic, M. Marinelli, in *Analytical Sciences/Supplements Proc. of 11th Int. Conf. of Photoacoustic and Photothermal Phenomen*, Japan, **2002**, pp. s185–s188.
- [13] M. Chirtoc, N. Horny, *J. Appl. Phys.* **2022**, *131*, 214502.
- [14] P. Martínez-Torres, J. J. Alvarado-Gil, *Appl. Phys. A*, **2011**, *105*, 975.
- [15] N. W. Pech-May, J. J. Alvarado-Gil, *Rev. Sci. Instrum.* **2013**, *84*, 084902.
- [16] J. May-Crespo, P. Martinez-Torres, J. J. Alvarado-Gil, P. Quintana, J. Ordonez, *Int. J. Thermophys.* **2010**, *31*, 1027.
- [17] M. Vargas-Luna, G. Gutiérrez-Juárez, J. M. Rodríguez-Vizcaíno, J. B. Varela-Nájera, J. M. Rodríguez-Palencia, J. Bernal-Alvarado, J. J. Alvarado-Gil, *J. Phys. D: Appl. Phys.* **2002**, *35*, 1532.
- [18] Z. Hua, R. Schley, D. Hurley, *Rev. Sci. Instrum.* **2022**, *93*, 044903.
- [19] X. Fan, W. Nie, H. Tsai, N. Wang, H. Huang, Y. Cheng, Y. Xia, *Adv. Sci.* **2019**, *6* 1900813.
- [20] Thermtest Inc., Materials Thermal Properties Database, <https://thermtest.com/thermal-resources/materials-database>.
- [21] A. P. Franco-Bacca, F. Cervantes-Alvarez, J. D. Macías, J. A. Castro-Betancur, R. J. Pérez-Blanco, O. H. Giraldo Osorio, J. J. Alvarado-Gil, *Polymers* **2021**, *13*, 4106.
- [22] H. D. Özeren, M. Guivier, R. T. Olsson, F. Nilsson, M. S. Hedenqvist, *ACS Appl. Polym. Mater.* **2020**, *2*, 2016.
- [23] A. Mandelis, *Chem. Phys. Lett.* **1984**, *108*, 388.
- [24] A. Landa, J. J. Alvarado-Gil, J. Gutiérrez-Juárez, M. Vargas-Luna, *Rev. Sci. Instrum.* **2003**, *74*, 377.
- [25] N. Horny, M. Chirtoc, A. Fleming, G. Hamaoui, H. Ban, *Appl. Phys. Lett.* **2016**, *109*, 033103.
- [26] J. A. Balderas-López, A. Mandelis, *J. Appl. Phys.* **2001**, *90*, 2273.
- [27] A. J. Schmidt, R. Cheaito, M. Chiesa, *Rev. Sci. Instrum.* **2009**, *80*, 094901.
- [28] S. Kasap, D. Tonchev, *Thermal Properties and Thermal Analysis*, Springer Handbooks. Springer, Boston, MA, **2006**.
- [29] The International Centre for Diffraction Data, Powder Diffraction File (PDF) Search. <https://www.icdd.com/pdfsearch/>.
- [30] O. V. Malyshkina, A. A. Movchikova, O. N. Kalugina, A. V. Daineko, *Ferroelectrics* **2011**, *424*, 28.
- [31] X. Zhang, C. P. Grigoropoulos, *Rev. Sci. Instrum.* **1995**, *66*, 1115.
- [32] T. Yamane, Y. Mori, S. I. Katayama, M. Todoki, *J. Appl. Phys.* **1997**, *82*, 1153.
- [33] J. A. Ramírez-Rincón, O. Ares-Muzio, J. D. Macias, M. A. Estrella-Gutiérrez, F. I. Lizama-Tzec, G. Oskam, J. J. Alvarado-Gil, *J. Appl. Phys. A* **2018**, *124*, 252.
- [34] G. Hamaoui, N. Horny, C. L. Gomez-Heredia, J. A. Ramirez-Rincon, J. Ordonez-Miranda, C. Champeaux, F. Dumas-Bouchiat, J. J. Alvarado-Gil, Y. Ezzahri, K. Joulain, M. Chirtoc, *Sci. Rep.* **2019**, *9*, 8728.